HHS Public Access

Author manuscript

Biochemistry. Author manuscript; available in PMC 2017 July 07.

Published in final edited form as:

Biochemistry. 2017 May 02; 56(17): 2338–2348. doi:10.1021/acs.biochem.7b00165.

Hydrogen/Deuterium Exchange Mass Spectrometry of Human Green Opsin Reveals a Conserved Pro-Pro Motif in Extracellular Loop 2 of Monostable Visual G Protein-Coupled Receptors

Lukas Hofrnann, **Nathan S. Alexander**, **Wenyu Sun**, **Jianye Zhang**, **Tivadar Orban**[*], and **Krzysztof Palczewski**[*]

Department of Pharmacology and Cleveland Center for Membrane and Structural Biology, School of Medicine, Case Western Reserve University, 10900 Euclid Avenue, Cleveland, Ohio 44106, United States

Abstract

Opsins comprise the protein component of light sensitive G protein-coupled receptors (GPCRs) in the retina of the eye that are responsible for the transduction of light into a biochemical signal. Here, we used hydrogen/deuterium (H/D) exchange coupled with mass spectrometry to map conformational changes in green cone opsin upon light activation. We then compared these findings with those reported for rhodopsin. The extent of H/D exchange in green cone opsin was greater than in rhodopsin in the dark and bleached states, suggesting a higher structural heterogeneity for green cone opsin. Further analysis revealed that green cone opsin exists as a dimer in both dark (inactive) and bleached (active) states, and that the predicted glycosylation sites at N^{32} and N^{34} are indeed glycosylated. Comparison of deuterium uptake between inactive and active states of green cone opsin also disclosed a reduced solvent accessibility of the extracellular N-terminal region and an increased accessibility of the chromophore binding site. Increased H/D exchange at the extracellular side of transmembrane helix four (TM4) combined with an analysis of sequence alignments revealed a conserved Pro-Pro motif in extracellular loop 2 (EL2) of monostable visual GPCRs. These data present new insights into the locus of chromophore release at the extracellular side of TM4 and TM5 and provide a foundation for future functional evaluation.

[*]Corresponding Authors: Department of Pharmacology, School of Medicine, Case Western Reserve University, 10900 Euclid Ave., Cleveland, OH 44106-4965. Phone: 216-368-8794. Fax: 216-368-1300. txo54@case.edu. [*]Department of Pharmacology, School of Medicine, Case Western Reserve University, 10900 Euclid Ave., Cleveland, OH 44106-4965. Phone: 216-368-4631. Fax: 216-368-1300. kxp65@case.edu.

Supporting Information: The Supporting Information is available free of charge on the ACS Publications website at DOI: 10.1021/acs.bio-chem.7b00165. Sequence alignment of green opsin and the green opsin construct used in this study; detailed regeneration, protein purification, and immunoblotting protocols for the green cone opsin; analysis of the oligomeric state by gel filtration and native PAGE of the green cone opsin; a detailed description of the peptide detection and H/D exchange analysis, including the H/D exchange analysis and normalization (Table S1); sequence alignment of the green opsin construct, L/LWS opsin, bovine rhodopsin, and SWS1 opsin; sequence alignment excerpt of conserved Pro residues in pigments from different species; quantitative RMSD analysis of green opsin, P205I, and P186 mutants; sequence alignment of green opsin, 5-HT_{1B}, and 5-HT_{2B} receptors; and nonoverlapping local alignment of 5-HT_{1B} receptor and green opsin sequences (PDF)

Notes: The authors declare no competing financial interest.

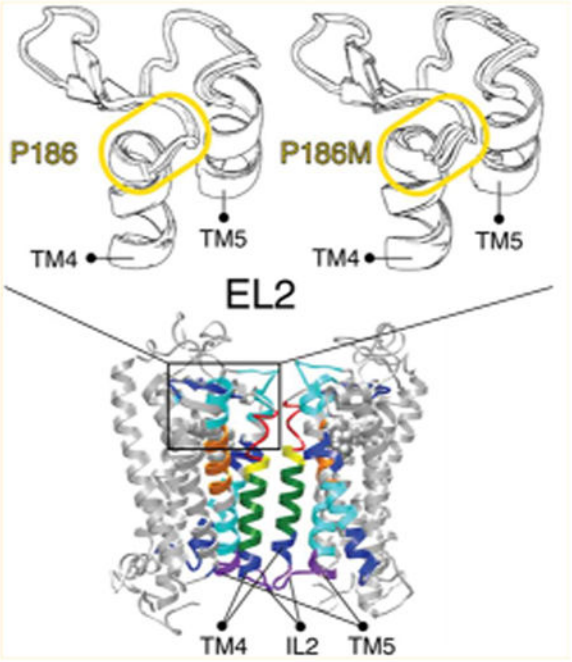

Opsins are an essential part of the visual sensory system that function as photon detectors in the retina.[1,2] The four opsins in the human retina [rhodopsin, short wavelength sensitive 1 (SWSl) opsin, medium wavelength sensitive 1 (M/LWS) opsin, and long wavelength sensitive 1 (L/LWS) opsin] differ in their spectral absorbance, sensitivity, regeneration kinetics, and regulation of downstream signaling.[3,4] All four pigments are activated by the isomerization of the chromophore 11-*cis*-retinal to all-*trans*-retinal, which is then released and regenerated back to 11-*cis*-retinal through the retinoid cycle.[5] Chromophore photoisomerization induces conformational changes in these light sensitive GPCRs and initiates the binding of the G proteins, transducins.[6–8] The two different conformational states, active and inactive, are known to be very stable and discrete in rhodopsin.[8] However, most GPCRs display different and more heterogeneous states that permit biased signaling and different active states induced by different ligands.[9–11] Ongoing difficulties associated with GPCR crystallization have prevented the experimental determination of the atomic structures for SWSl, M/LWS, and L/LWS opsins. Therefore, understanding the structural underpinnings of their functional differences remains a challenge.

GPCRs in general can exist as functional monomers, homo/heterodimers, or even higher oligomeric species.[12–14] Different oligomeric organizations may affect signaling and other physiological properties of these receptors and can, therefore, serve as distinct targets for drug screens.[15,16] Opsins are known to form homodimers and higher oligomeric structures, as shown by cryo-electron microscopy, atomic force microscopy, and fluorescence assays.[12,14,17] Disruption of the oligomeric organization of bovine rhodopsin with synthetic peptides confirmed that the dimer interface is located between TM4 and TM5.[18] Recent analyses of the human M/LWS, L/LWS, and SWSl cone opsins by fluorescence correlation spectroscopy also revealed a dimer interface between TM4 and TM5 in human cone pigments.

Visual pigments can be divided into two types: monostable forms, which release the chromophore upon photoactivation, and bistable forms, which retain the chromophore within the binding pocket.[19–21] A subset of bistable opsins can re-isomerize the chromophore.[19,20] For re-isomerization, the chromophore must remain within the binding pocket. Mutagenesis studies of chicken rhodopsin and chicken green cone opsin revealed that Prol89 in EL2 has a crucial impact on the meta-II and meta-III decay rates. Prol89 is conserved in cone opsins but not rhodopsins, which suggests that residues within EL2 likely influence chromophore release in monostable opsins.[22,23] Additionally, evaluation of the backbone configuration based on 500 high-resolution protein crystal structures has shown a restricted conformational freedom of Pro and residues preceding Pro.[24,25] This geometrical restriction originates from the pyrrolidine ring of Pro. Moreover, Pro residues found in transmembrane domains are known to induce helix kinks that are indispensable for the integrity of the transmembrane helices.[26] Additionally, molecular dynamics simulations of α-helical transmembrane proteins (e.g., GPCRs) showed that Pro-induced hinges play a crucial role in signal transduction.[27,28] Thus, the conformational restriction and impact on α-helical structure reinforce the selection of Pro residues as switches for binary signaling triggered by the *cis-trans* isomerization of retinal in rhodopsin and cone opsins.[29]

H/D exchange measurements are used to probe protein dynamics and protein-ligand interactions, providing information complementary to other structural techniques such as nuclear magnetic resonance spectroscopy (NMR), X-ray crystallography, cryo-electron microscopy, and computational modeling.[30–33] H/D exchange reflects the exposure of residues to the surrounding environment and depends on several parameters such as temperature, pH, ionic strength, exposure time, and hydrogen bonding. With careful experimental control of these first four parameters, detection of changes in secondary and tertiary structure and protein dynamics is possible.[31,33] Because of solvent exchange, this method is especially suited for GPCR analysis, considering the conserved hydrogen bond network involving water molecules that exists throughout this group.[34,35] Here, we looked specifically at H/D exchange in the dark and bleached states of M/LWS (green) cone opsin.

Materials and Methods

Cloning, Expression, and Protein Purification

The human green opsin gene (Uniprot entry P04001) was modified with a 1D4 tag in the C-terminal region.[36] This construct was cloned into a modified pFastBac (Invitrogen, Carlsbad, CA) baculovirus expression vector containing the hemeagglutinin (HA) signal sequence.

The modified green opsin construct was transformed into DH10Bac to produce a recombinant baculovirus with the Bac-to-Bac system (Invitrogen). This recombinant baculovirus then was used to infect an Sf9 insect cell culture at a cell density of 3×10^6 cells/mL. Infected cells were grown for 60 h at 27 °C before being harvested, and cell pellets were stored at -80 °C for future use. A detailed protocol for regeneration and solubilization of the green cone pigment in *n*-dodecyl β-D-maltopyranoside (DDM) is presented in the Supporting Information.

The purity of the green cone opsin after size exclusion chromatography (SEC) in 20 mM HEPES (pH 7.0), 50 mM NaCl, and 0.02% DDM was assessed by sodium dodecyl sulfate-polyacrylamide gel electrophoresis (SDS-PAGE) and spectrophotometry (Figure 1A-D). The reported extinction coefficient for the green photopigment (ε530) equals 40000 M^{-1} cm^{-1}, and the calculated ε_{280} equals 99975 M- cm^{-1}.[37] Thus, a theoretical ratio (A_{280}/A_{530}) of 2.49 would indicate a pure sample. Here we obtained an A_{280}/A_{530} of 2.86, which together with the data obtained by SDS-PAGE indicates a purity close to 100%

Rhodopsin purity is assessed by comparing the ratios of the absorption maxima at 280 nm (aromatic amino acid residues) and 500 nm (bound chromophore) in the dark. This A_{280}/A_{500} ratio for purified rhodopsin varies between 1.58 and 1.65, reflecting a purity of ~99%.[38]

Differential Scanning Fluorimetry

Protein stability was assessed by differential scanning fluorimetry as previously reported.[39] Briefly, bovine rhodopsin (Uniprot entry P02699) and the green pigment were diluted in 20 mM HEPES (pH 7.0), 50 mM NaCl, and 0.02% DDM to a concentration of 6 μM and assayed in the presence of 2 μM reporter dye, BODIPY FL L-cystine (ThermoFisher, Waltham, MA). Melting temperatures were determined in triplicate using a Boltzmann fit performed with SigmaPlot version 11.0.

Amide H/D Exchange of Green Opsin

Amide H/D exchange was performed and analyzed as described previously.[40–42] Briefly, 10 μg of purified green pigment in 20 mM HEPES (pH 7.0), 50 mM NaCl, and 0.02% DDM was diluted in 25 μL of D_2O, resulting in a final D_2O dilution of 80%. The solution was kept on ice and incubated for 10 min. This D_2O exposure time (i.e., 10 min) was chosen to achieve steady state exchange conditions so deuterium uptake in each peptide could be compared between states (dark vs bleached) without the need to evaluate back exchange and have only one parameter that changes between states, i.e., light. To initiate chromophore release, the sample was placed on ice and illuminated with a 150 W bulb for 30 min before incubation in D_2O.[34] The incubation time in D_2O was tested and optimized using data from hundreds of peptides following protocols from similar experiments in which the dilution was kept at 80%.[30,43–46] After exposure to D_2O, the exchange was quenched with ice-cold buffer composed of D_2O and formic acid (Sigma-Aldrich, St. Louis, MO) at pH 2.5. The quenching buffer used in the nondeuterated samples was prepared with H_2O. Pepsin (Worthington, Lakewood, NJ), 2.5 mg/mL, was freshly prepared in H_2O for both deuterated and nondeuterated samples. Five microliters were added to the protein solution immediately after addition of the quenching buffer. The sample then was digested for 5 min on ice. Next, the sample (30 μL) was loaded onto a C8 trap (2.1 mm Thermo Scientific) and a C4 (2.1 mm × 50 mm, Thermo Scientific) column using a temperature-controlled Accela 600 autosampler and pump (Thermo Scientific) with the temperature set to 4 °C. Peptides were eluted by the following gradient program: from 98% H_2O with 0.1% (v/v) formic acid (A) and 2% acetonitrile with 0.1% (v/v) formic acid (B) from 0 to 40 min to 2% A and 98% B. Separation was achieved at a flow rate of 0.1 mL/min. The eluent was injected into a LTQ Velos linear trap quadropole mass spectrometer (Thermo Scientific) equipped with an

electrospray ionization source operated in positive ion mode. Parameter settings of the mass spectrometer for peptide detection are provided in the Supporting Information.

Deglycosylation of Green Opsin by PNGase F Digestion

Purified green opsin was incubated with PNGase F at 22 °C for 2 h prior to SDS-PAGE. The effect of PNGase F digestion was monitored by SDS-PAGE and immunoblotting analysis (see Figure 1C,D and the Supporting Information).

Analysis of H/D Exchange

Peptides resulting from pepsin digestion were identified by tandem mass spectrometry (MS/MS) with an offline local version of MassMatrix.[47] Search settings used to examine the peptic digest against the primary sequence of human green opsin construct (see the Supporting Information) were as follows: precursor ion tolerance, 0.8 Da; maximal number of variable modifications allowed for each peptide sequence, 2; minimal peptide length, 5 amino acids; minimal pp score, 5; pp_{tag} score, 1.3; maximal number of combinations of different modification sites for a peptide match with modifications, 1; and maximal number of candidate peptide matches for each spectrum output in the result, 1.[48] Raw data in the form of the relative signal intensity (percent) as a function of m/z were extracted with Xcalibur version 2.1.0. Qual Browser was used for a recently described semiautomated peak detection, and a deconvolution procedure was performed with HX-Express^2.[49] The extent of H/D exchange was color-coded on the basis of the total percent of the theoretical maximal deuterium uptake at 10 min as follows: dark blue for 0–4%, light blue for 5–9%, cyan for 10–14%, cadet blue for 15–19%, green for 20–24%, light green for 25–29%, yellow for 30–34%, orange for 35–39%, and red for 40–44%. Undefined regions are colored gray. In the case of overlapping peptides, the percentage of H/D exchange applied is shown with a solid line (Figure 2A). For gaps in the coverage, the missing percentage was derived from peptides with a dashed line (Figure 2A). The difference map of Figure 3 contains only identical peptides, found in both states (dark and bleached). Further details of the H/D exchange analysis are given in the Supporting Information.

Green Opsin Modeling

A model of the human green cone opsin was created with the 2.2 Å resolution crystal structure of rhodopsin [Protein Data Bank (PDB) entry 1U19]. The EMBOSS Needle Pairwise Sequence Alignment tool was used to align the two sequences.[50] The MEDELLER server generated an initial structure for the green cone opsin based on the sequence alignment.[51] The resulting MEDELLER structure then was used as input into the ROSETTA protein structure prediction suite, where the conformation of the 20 N-terminal amino acids was sampled 60 times with the loop building protocol and the best model by energy was selected.[52]

Single-Point Mutations of Green Opsin (P186M and P205I)

Two single-point mutations in green opsin were created with ROSETTA. The mutations P186M and P205I were introduced into the green opsin model with the fixed backbone design module of ROSETTA.[53] Next, all models underwent 1000 independent full-structure

optimization trajectories in ROSETTA employing the membrane fast relax protocol.[54] The 10 most energetically favorable structures for each of the three models (green pigment, P186M, and P205I) were then selected for further analysis. Ten energetically favored models of WT and the two mutants were aligned with PyMOL.[55] Root-mean-square deviation (RMSD) analysis between these aligned structures was performed with the VMD RMSD Visualizer Tool heatmapper extension.[56]

Statistical Analyses

Graphical and statistical analyses were performed using the Excel software part of the Microsoft Office Professional 2010 suite if not indicated otherwise. Significance was assessed using a Student's *t* test, and results that showed *p* values of <0.01 were considered significant. The data were derived from at least three independent experiments.

Results

Green Opsin Dynamics from H/D Exchange

The MS/MS spectra of the green opsin digest were analyzed with MassMatrix software based on the primary sequence of the L/MWS construct (see the Supporting Information).[57] A sequence coverage of 94.7% was achieved for the deuterated green pigment protein (Figure 2A) by rigorous screening and selection of only significant peptide matches (see Materials and Methods and the Supporting Information for details). The deuteration of the green opsin ranged from 1 to 50%, which agrees with H/D exchange values of other GPCRs.[30,41,58]

Overall, there was an increase in the uptake of deuterium in the bleached state compared with the dark state of the green photopigment. The difference map of H/D exchange between dark and bleached states revealed several major changes upon light activation (Figure 3). First, the chromophore binding pocket became more solvent accessible during activation (Figure 3A), indicating a potential exit site for all-*trans*-retinal (Figure 3A,B,E). The increased deuterium uptake started at TM1 and extended over TM2 and TM3 (Figure 3A,D). The largest increase in deuterium uptake within the region of the binding pocket was observed on the extracellular side of TM4 (Figure 3). In contrast, the proposed dimer interface consisting of TM4 and TM5 was characterized by an overall reduced level of deuterium exchange compared to the rest of the pigment molecule (Figures 3B and 4).[17] The dimeric state of the green pigment was further assessed by size exclusion chromatography (SEC) and native PAGE (Figure S1). SEC experiments revealed a molecular weight (MW) of 99284 Da for the green opsin. This molecular weight corresponds to a dimer (81 kDa) with an additional detergent belt of approximately 18 kDa (Figure S1). Similar findings regarding the dimeric state of the cone pigments have been reported.[17] The N-terminal region and intracellular loop 2 (IL2) also showed less deuterium exchange in the bleached state of the photopigment (Figure 3A,B,F); the largest reduction in deuterium uptake was observed for the N-terminal region (Figure 3A,C,E). Extracellular loops (ELs) 1–3 exhibited little difference in deuterium uptake.

Only TM1 to TM4 of the green opsin underwent a significant increase in deuterium uptake upon activation (Figure 3A). Again, we saw an increased level of H/D exchange along the chromophore binding pocket. In contrast, the H/D exchange levels of TM5 remained constant upon activation. Moreover, the cytosolic parts of TM6 and TM7 demonstrated a decrease in H/D exchange in the active conformation (Figure 3E). Overall, the highest but constant level of deuterium uptake was observed in the extracellular parts of TM6 and TM7, including EL3 (Figures 3E and 4A). These large exchanges were observed in both dark and bleached states (Figures 3E and 4A).

As reported previously, the dimer interface of green opsin was localized between TM4 and TM5, with residues T230, S233, and V236 of TM5 being crucial for dimerization.[17] The dimer interface between two species of green opsin revealed two major changes upon activation (Figure 4). First, there was an increase in H/D exchange at the tip of the chromophore binding pocket located at TM4 on the extracellular side (Figure 4A,E). Second, a decrease in H/D exchange was observed in IL2 (Figure 4B,D). In addition, both IL2s were in proximity of each other between the dimer interface (Figure 4D). The reduced H/D exchange of IL2 and the location at the dimer interface of the green pigment indicates a potential role of IL2 in green opsin signaling influenced by dimerization.

Glycosylation of the Green Photopigment

Previous analysis of the green photopigment expressed in Sf9 insect cells showed evidence of N-linked glycosylation, although the prediction was not confirmed experimentally.[37] Here, glycosylation was validated by SDS–PAGE and immunoblotting analysis. PNGase F-treated pigment displayed a migration shift (Figure 1C,D), resulting from the deglycosylation of the green opsin. Additionally, the sites of glycosylation were verified by MS. Glycosylation is lost during ionization, and therefore, glycosylated asparagine residues are converted to aspartate. Consequently, asparagine-linked glycosylation can be identified by assuming N to D transformations during the MS/MS analysis (Figure 2A,B). Potential glycosylation sites of the green cone pigment were predicted with the NetNGlyc 1.0 Server prior to MS analysis.[59] The top three asparagine residues with a glycosylation prediction score of >0.71 out of 1 (i.e., N32, N34, and N94) were verified by MS/MS. The predicted glycosylation sites, N32 and N34, were confirmed by the MS/MS analysis of peptide ^{29}TYTDSDSTRGPGENGPNY^{46} (Figure 2B). A third glycosylation site (N94) with a prediction score of 0.78 was indicated by the server but was not confirmed by mass spectrometry.

Computational Modeling

The H/D exchange data indicate a rearrangement of EL2 between the dark and bleached states of green opsin, suggesting a possible role in chromophore exchange. EL2 contains a Pro-Pro motif conserved across all monostable but not bistable visual pigment proteins (see the Supporting Information). To further characterize the structural effect of this motif, a model of green opsin containing a single substitution, P186M, was compared to the green pigment model. Analyzing the 10 most energetically favorable structures resulting from independent optimization trajectories for both the green pigment and P186M models demonstrated that the P186M model had increased flexibility at the end of TM4 as

compared to the green pigment model (compare Figure 5A,B,D and Figure S2). The increased flexibility in TM4 induced by the P186M mutation agrees with the reduction of the number of geometric constraints induced by the exchange of a Pro residue. The region of increased flexibility corresponds to the site of increased deuterium uptake after photon-activation of green cone opsin (Figures 3A,D and 4). To verify that our modeling can identify structural changes with functional consequences from a singleamino acid substitution, we also prepared a model with a P205I point mutation in green opsin. P205I was previously shown to affect the meta-II and meta-III decay rates in chicken green cone opsin.[22,23,60] Comparison of the structural ensembles between the P205I and green pigment models demonstrated an increased flexibility at the C-terminal region of EL2 in the P205I model, consistent with changes in the decay rates of meta conformers (compare Figure 5A,C,D and Figure S2). These data demonstrate that results from the computational modeling and RMSD analysis presented here agree with those of mutagenesis studies that describe chromophore release in visual opsins.[22,23,60]

Discussion

We previously reported an H/D exchange analysis of bovine rhodopsin.[30] Herein, we provide an H/D exchange analysis of the inactive and active states of green cone pigment and compare these findings with those for rhodopsin.[30] Overall, the differences between the inactive and active states observed in the green visual pigment and rhodopsin ranged from −25 to 15% and from −50 to 40%, respectively. These differences indicate that the two states are more distinct in rhodopsin than in green cone opsin. It should be noted, however, that the analysis of the N-terminal region, IL1, IL2, and TM5 is lacking in the rhodopsin model because of low coverage. A reduced level of deuterium uptake upon bleaching in TM1 is common to both rhodopsin and the green pigment. In addition, the increased level of deuterium exchange along the chromophore binding pocket is found in both pigments. Also in rhodopsin, the H/D exchange rate in the chromophore binding pocket peaks at the extracellular side of TM4. In green cone opsin, we measured a reduced level of H/D exchange in IL2 upon activation, and the same is true for rhodopsin. Rhodopsin shows an increased level of H/D exchange in TM3 and a decreased level of exchange in IL3. These differences were not detected in green opsin. In green opsin, we detected an overall decrease in the H/D exchange rate for TM6 and TM7 upon activation. Bovine rhodopsin displays a reduced exchange rate in TM6 but not in TM7.[30]

Extensive research on the role of the extracellular loops (ELs) in GPCRs has demonstrated that ELs are involved in ligand recognition and binding and can function as gatekeepers in GPCR signaling.[61–63] GPCR structural studies demonstrated a high variability in the sequence and length of the ELs.[61,62,64] The ELs of light sensitive GPCRs play a unique role. Unlike other GPCRs, which are activated by molecules, opsins are activated by light.[65,66] Thus, attention has focused on the potential role of the ELs in rhodopsin, because of the absence of a direct ligand interaction and their role in chromophore release.[67] NMR studies combined with crystallographic data about rhodopsin offered valuable insights into the motion of EL2 following activation.[67,68] EL2 forms a lid on the retinal binding site and interacts directly with the chromophore.[69,70] Photoactivation displaces EL2 in rhodopsin and rearranges the hydrogen bond network.[71] Displacement of EL2 along with TM4-TM6

involves a conserved hydrogen bond network stretching throughout rhodopsin.[35,67] Thus, interactions among these components are critical for opsin activation and chromophore release. Comparable studies of cone opsins have not been reported to date.

The extracellular N-terminal region of green opsin is 18 amino acid residues longer than the corresponding region of rhodopsin (see the Supporting Information). Mutagenesis experiments and molecular dynamics studies of the *Xenopus* violet cone pigment revealed a hydrogen bonding network among the N-terminal region, EL2, and EL3. In rhodopsin, EL3 builds a hydrogen network with the N-terminal region but not with EL2. These differences in the hydrogen network at the extracellular site between cone opsins and rhodopsin provide a possible explanation for the decreased H/D exchange upon receptor activation.[72,73]

Thermal unfolding of bovine rhodopsin and green opsin was monitored by differential scanning fluorimetry (Figure 1E).[39] The melting temperatures were found to be 48 and 72 °C for green opsin and rhodopsin, respectively. The melting temperature difference of 24 °C indicates a reduced stability of green opsin, which is in agreement with other class A GPCRs such as the human CB1 cannabinoid receptor.[74] Unlike rhodopsin, most GPCRs are inherently unstable and express multiple ligandspecific active states.[9,10,75] Successful crystallization of rhodopsin in its active and inactive states without stabilizing agents, signaling partners, or antibodies suggests that both states are discrete and do not suffer from inherent instability and multiple heterogeneous states.[76,77] The reduced stability of green cone pigment indicates higher mobility of the protein domains and thus an increased overall solvent exposure. Increased solvent exposure reduces the differences in H/D exchange between different states, such as the dark and bleached states of green cone opsin. This difference in stability of green opsin versus rhodopsin complicates a direct comparison by state between these two light sensitive pigments.

We provide experimental data suggesting a potential exit site for the photoisomerized chromophore, all-*trans*-retinal, between TM4 and TM5 at the extracellular surface of green opsin (Figure 6). The increased H/D exchange upon bleaching at the chromophore binding pocket domain is most prominent at the extracellular side of TM4. Moreover, the exit site between TM4 and TM5 is favored in dark state rhodopsin, based on molecular dynamics simulations.[78] However, similar calculations on the bleached state of bovine rhodopsin and mutagenesis studies provide evidence that the exit site resides between TM5 and TM6, a finding we were unable to recapitulate for green opsin in our H/D exchange experiments.[79–81]

Alignment analysis of monostable visual opsin protein sequences from different species revealed a conserved Pro186-Pro187 sequence at TM4 (see the Supporting Information). This conserved Pro-Pro motif coincides with the site of largest difference in H/D exchange upon photoactivation of the green cone pigment. Additionally, it was previously proposed that the Pro170 and Pro171 residues in bovine rhodopsin are involved in accommodating the perturbation of the helix upon receptor activation.[82,83] Also, single mutations P170H and P171S in rhodopsin can cause retinitis pigmentosa in humans.[84,85] Interestingly, bistable pigments that do not release the chromophore (e.g., human Opn5 and visual bistable opsins of Drosophila melanogaster and Todarodes pacificus) contain only a single conserved Pro

residue at TM4 (see the Supporting Information).[86] Taken together, these data show that the presence of the Pro-Pro motif is crucial for a fully functional monostable visual opsin.

5-Hydroxytryptamine receptor 1B (5-HT_{1B}) is the only crystallized GPCR (PDB entries 4IAQ and 4IAR) besides rhodopsin that contains a Pro-Pro motif at TM4. The 5-HT_{1B} receptor has a sequence similarity of 65% with the green pigment at the Pro-Pro site of TM4 (Figure S3). Comparison of the green cone pigment model with the 5-HT_{1B} structure revealed an alternative and extended TM4 and EL2 of 5-HT_{1B}.[87,88] Furthermore, recent data regarding the 5-hydroxytryptamine receptor 2B receptor combined with molecular dynamics simulations highlight the crucial role of the EL2 site in ligand binding.[63] These data support the possibility that the conserved Pro-Pro motif in TM4, including the EL2 in vertebrate visual opsins, is involved in chromophore release.

RMSD analysis of the energetically favored structures revealed that the P205I mutation increases the structural flexibility in the TM4–EL2–TM5 region compared to the WT. Previous in vitro mutagenesis experiments showed that this mutation prolongs the meta-III decay rate. Taken together, these results suggest that the increased structural variability is related to the delayed chromophore release. A similar pattern of increased flexibility is observed in the TM4–EL2–TM5 region of the P186M mutant. In addition, all monostable pigments contain a Pro-Pro motif in the TM4–EL2–TM5 region, compared to a single Pro for bistable pigments, which further suggests P186 and the TM4–EL2–TM5 region can affect chromophore release. Characterizing the role of the TM4–EL2–TM5 region in chromophore release is one interesting direction for future studies.

It remains unclear whether all-*trans*-retinal is released through TM4 and TM5 or if relaxation or helix unwinding of TM4 serves as a water counterbalance valve, as found in other hydrophobic ligand transport proteins.[89,90] Changes in the solvent accessibility at TM4 could also alter the solvent network within GPCRs, which impacts the continuous H-bond network contributing to G protein activation and thus regulates GPCR activity.[35,91–94]

Herein, we provide further evidence that supports the proposed dimer interface of green opsin (Figure 4).[17] This dimer interface between TM4 and TM5 exhibits a reduced level of H/D exchange, compared to those of other TM domains (Figure 4). We also observed a reduction of H/D exchange in IL2 upon receptor activation, whereas the remaining ILs did not exhibit significant changes (Figure 3F). Residing at the dimer interface between TM4 and TM5 (Figure 4), IL2 directly interacts with Gα and β-arrestin and thus is crucial for G protein signaling and desensitization.[8,95] Thus, stabilization of IL2 through dimerization could potentially affect interactions with these signaling proteins and cause an altered activation state of the receptor.[8,96] The question of whether stabilization of IL2 leads to prolonged activation through increased G protein interaction and reduced affinity for arrestin or faster desensitization through weakened G protein interaction and increased affinity for arrestin remains to be answered.[96]

In summary, we employed H/D exchange coupled with MS, differential scanning fluorometry, bioinformatics, and computational modeling to investigate dynamic structural changes in green opsin that occur upon photoactivation and chromophore release. Post-

translational modifications of GPCRs play critical roles in protein folding, transport, and signaling.[97,98] In bovine rhodopsin, N-terminal glycosylation has been studied extensively, and its importance in trafficking and signaling has been demonstrated.[99,100] It was previously proposed that green cone opsin, expressed in Sf9 insect cells, is glycosylated at its N-terminal region like rhodopsin, but confirmation of this has been lacking.[37] The MS/MS analysis of green opsin reported here verified the proposed N-terminal glycosylation at asparagine residues 32 and 34. Future studies with alternative deglycosylation enzymes such as PNGase A can be applied to further explore the role and pattern of glycosylation in receptor dynamics. H/D exchange analysis also revealed a Pro-Pro motif with an increased level of exchange upon photoactivation and chromophore release. Sequence alignment of monostable and bistable opsins revealed that the Pro-Pro motif is conserved in all monostable opsins but does not occur in bistable opsins, suggesting a role of TM4 in chromophore release. In addition, computational analysis indicated that the P186M substitution, as seen in bistable proteins, permits greater conformational flexibility, further implicating TM4 and EL2 in the process of chromophore release in monostable visual opsins.

Supplementary Material

Refer to Web version on PubMed Central for supplementary material.

Acknowledgments

L.H. is supported by a Swiss National Science Foundation Doc.Mobility Fellowship (P1SKP3_158634). This work was supported by funding from National Institutes of Health Grants EY025007 (N.S.A), EY009339 (K.P.), and EY027283 (K.P.), the Arnold and Mabel Beckman Foundation, and the Canadian Institute for Advanced Research. K.P. is the John Hord Professor of Pharmacology. We thank Dr. Leslie T. Webster, Jr., and members of the Palczewski laboratory for helpful comments regarding the manuscript.

References

1. Bowmaker JK. Evolution of vertebrate visual pigments. Vision Res. 2008; 48:2022–2041. [PubMed: 18590925]
2. Hofmann L, Palczewski K. Advances in understanding the molecular basis of the first steps in color vision. Prog Retinal Eye Res. 2015; 49:46–66.
3. Imamoto Y, Shichida Y. Cone visual pigments. Biochim Biophys Acta, Bioenerg. 2014; 1837:664–673.
4. Korenbrot JI. Speed, sensitivity, and stability of the light response in rod and cone photoreceptors: facts and models. Prog Retinal Eye Res. 2012; 31:442–466.
5. Kiser PD, Palczewski K. Retinoids and Retinal Diseases. Annu Rev Vis Sci. 2016; 2:197–234. [PubMed: 27917399]
6. Jastrzebska B, Ringler P, Lodowski DT, Moiseenkova-Bell V, Golczak M, Muller SA, Palczewski K, Engel A. Rhodopsin-transducin heteropentamer: three-dimensional structure and biochemical characterization. J Struct Biol. 2011; 176:387–394. [PubMed: 21925606]
7. Kobilka BK. G protein coupled receptor structure and activation. Biochim Biophys Acta, Biomembr. 2007; 1768:794–807.
8. Rosenbaum DM, Rasmussen SG, Kobilka BK. The structure and function of G-protein-coupled receptors. Nature. 2009; 459:356–363. [PubMed: 19458711]
9. Steyaert J, Kobilka BK. Nanobody stabilization of G protein-coupled receptor conformational states. Curr Opin Struct Biol. 2011; 21:567–572. [PubMed: 21782416]

10. Heydenreich FM, Vuckovic Z, Matkovic M, Veprintsev DB. Stabilization of G protein-coupled receptors by point mutations. Front Pharmacol. 2015; 6:82. [PubMed: 25941489]
11. Zhang X, Stevens RC, Xu F. The importance of ligands for G protein-coupled receptor stability. Trends Biochem Sci. 2015; 40:79–87. [PubMed: 25601764]
12. Fotiadis D, Liang Y, Filipek S, Saperstein DA, Engel A, Palczewski K. Atomic-force microscopy: Rhodopsin dimers in native disc membranes. Nature. 2003; 421:127–128. [PubMed: 12520290]
13. Jastrzebska B. GPCR: G protein complexes–the fundamental signaling assembly. Amino Acids. 2013; 45:1303–1314. [PubMed: 24052187]
14. Gunkel M, Schoneberg J, Alkhaldi W, Irsen S, Noe F, Kaupp UB, Al-Amoudi A. Higher-order architecture of rhodopsin in intact photoreceptors and its implication for phototransduction kinetics. Structure. 2015; 23:628–638. [PubMed: 25728926]
15. Ferre S, Casado V, Devi LA, Filizola M, Jockers R, Lohse MJ, Milligan G, Pin JP, Guitart X. G protein-coupled receptor oligomerization revisited: functional and pharmacological perspectives. Pharmacol Rev. 2014; 66:413–434. [PubMed: 24515647]
16. Chen Y, Palczewski K. Systems Pharmacology Links GPCRs with Retinal Degenerative Disorders. Annu Rev Pharmacol Toxicol. 2016; 56:273–298. [PubMed: 25839098]
17. Jastrzebska B, Comar WD, Kaliszewski MJ, Skinner KC, Torcasio MH, Esway AS, Jin H, Palczewski K, Smith AW. A G Protein-Coupled Receptor Dimerization Interface in Human Cone Opsins. Biochemistry. 2017; 56:61–72. [PubMed: 28045251]
18. Jastrzebska B, Chen Y, Orban T, Jin H, Hofmann L, Palczewski K. Disruption of Rhodopsin Dimerization with Synthetic Peptides Targeting an Interaction Interface. J Biol Chem. 2015; 290:25728–25744. [PubMed: 26330551]
19. Tsukamoto H, Terakita A. Diversity and functional properties of bistable pigments. Photochem Photobiol Sci. 2010; 9:1435–1443. [PubMed: 20852774]
20. Shichida Y, Matsuyama T. Evolution of opsins and phototransduction. Philos Trans R Soc B. 2009; 364:2881–2895.
21. Terakita A, Nagata T. Functional properties of opsins and their contribution to light-sensing physiology. Zool Sci. 2014; 31:653–659. [PubMed: 25284384]
22. Kuwayama S, Imai H, Morizumi T, Shichida Y. Amino acid residues responsible for the meta-III decay rates in rod and cone visual pigments. Biochemistry. 2005; 44:2208–2215. [PubMed: 15697246]
23. Kuwayama S, Imai H, Hirano T, Terakita A, Shichida Y. Conserved proline residue at position 189 in cone visual pigments as a determinant of molecular properties different from rhodopsins. Biochemistry. 2002; 41:15245–15252. [PubMed: 12484762]
24. Lovell SC, Davis IW, Arendall WB 3rd, de Bakker PI, Word JM, Prisant MG, Richardson JS, Richardson DC. Structure validation by Calpha geometry: phi,psi and Cbeta deviation. Proteins Struct Funct Genet. 2003; 50:437–450. [PubMed: 12557186]
25. Reimer U, Scherer G, Drewello M, Kruber S, Schutkowski M, Fischer G. Side-chain effects on peptidyl-prolyl cis/trans isomerisation. J Mol Biol. 1998; 279:449–460. [PubMed: 9642049]
26. Schmidt T, Situ AJ, Ulmer TS. Structural and thermodynamic basis of proline-induced transmembrane complex stabilization. Sci Rep. 2016; 6:29809. [PubMed: 27436065]
27. Sansom MSP, Weinstein H. Hinges, swivels and switches: the role of prolines in signalling via transmembrane alpha-helices. Trends Pharmacol Sci. 2000; 21:445–451. [PubMed: 11121576]
28. Elling CE, Frimurer TM, Gerlach LO, Jorgensen R, Holst B, Schwartz TW. Metal ion site engineering indicates a global toggle switch model for seven-transmembrane receptor activation. J Biol Chem. 2006; 281:17337–17346. [PubMed: 16567806]
29. Smith SO. Structure and activation of the visual pigment rhodopsin. Annu Rev Biophys. 2010; 39:309–328. [PubMed: 20192770]
30. Orban T, Jastrzebska B, Gupta S, Wang B, Miyagi M, Chance MR, Palczewski K. Conformational dynamics of activation for the pentameric complex of dimeric G protein-coupled receptor and heterotrimeric G protein. Structure. 2012; 20:826–840. [PubMed: 22579250]
31. Chalmers MJ, Busby SA, Pascal BD, West GM, Griffin PR. Differential hydrogen/deuterium exchange mass spectrometry analysis of protein-ligand interactions. Expert Rev Proteomics. 2011; 8:43–59. [PubMed: 21329427]

32. Lossl P, van de Waterbeemd M, Heck AJ. The diverse and expanding role of mass spectrometry in structural and molecular biology. EMBO J. 2016; 35:2634–2657. [PubMed: 27797822]
33. Jaswal SS. Biological insights from hydrogen exchange mass spectrometry. Biochim Biophys Acta, Proteins Proteomics. 2013; 1834:1188–1201.
34. Jastrzebska B, Palczewski K, Golczak M. Role of bulk water in hydrolysis of the rhodopsin chromophore. J Biol Chem. 2011; 286:18930–18937. [PubMed: 21460218]
35. Blankenship E, Vahedi-Faridi A, Lodowski DT. The High-Resolution Structure of Activated Opsin Reveals a Conserved Solvent Network in the Transmembrane Region Essential for Activation. Structure. 2015; 23:2358–2364. [PubMed: 26526852]
36. Molday LL, Molday RS. 1D4: a versatile epitope tag for the purification and characterization of expressed membrane and soluble proteins. Methods Mol Biol (NY NY US). 2014; 1177:1–15.
37. Vissers PM, DeGrip WJ. Functional expression of human cone pigments using recombinant baculovirus: compatibility with histidine tagging and evidence for N-glycosylation. FEBS Lett. 1996; 396:26–30. [PubMed: 8906860]
38. Salom D, Le Trong I, Pohl E, Ballesteros JA, Stenkamp RE, Palczewski K, Lodowski DT. Improvements in G protein-coupled receptor purification yield light stable rhodopsin crystals. J Struct Biol. 2006; 156:497–504. [PubMed: 16837211]
39. Hofmann L, Gulati S, Sears A, Stewart PL, Palczewski K. An effective thiol-reactive probe for differential scanning fluorimetry with a standard real-time polymerase chain reaction device. Anal Biochem. 2016; 499:63–65. [PubMed: 26851339]
40. Li S, Lee SY, Chung KY. Conformational analysis of g protein-coupled receptor signaling by hydrogen/deuterium exchange mass spectrometry. Methods Enzymol. 2015; 557:261–278. [PubMed: 25950969]
41. Zhang X, Chien EY, Chalmers MJ, Pascal BD, Gatchalian J, Stevens RC, Griffin PR. Dynamics of the beta2-adrenergic G-protein coupled receptor revealed by hydrogen-deuterium exchange. Anal Chem. 2010; 82:1100–1108. [PubMed: 20058880]
42. Orban T, Tsybovsky Y. Probing conformational changes in rhodopsin using hydrogen-deuterium exchange coupled to mass spectrometry. Methods Mol Biol (NY NY US). 2015; 1271:113–121.
43. Orban T, Bereta G, Miyagi M, Wang B, Chance MR, Sousa MC, Palczewski K. Conformational changes in guanylate cyclase-activating protein 1 induced by Ca2+ and N-terminal fatty acid acylation. Structure. 2010; 18:116–126. [PubMed: 20152158]
44. Tsybovsky Y, Orban T, Molday RS, Taylor D, Palczewski K. Molecular organization and ATP-induced conformational changes of ABCA4, the photoreceptor-specific ABC transporter. Structure. 2013; 21:854–860. [PubMed: 23562398]
45. Orban T, Huang CC, Homan KT, Jastrzebska B, Tesmer JJ, Palczewski K. Substrate-induced changes in the dynamics of rhodopsin kinase (G protein-coupled receptor kinase 1). Biochemistry. 2012; 51:3404–3411. [PubMed: 22480180]
46. Rajavel M, Orban T, Xu M, Hernandez-Sanchez W, de la Fuente M, Palczewski K, Taylor DJ. Dynamic peptides of human TPP1 fulfill diverse functions in telomere maintenance. Nucleic Acids Res. 2016; 44:10467–10479. [PubMed: 27655633]
47. Xu H, Freitas MA. MassMatrix: a database search program for rapid characterization of proteins and peptides from tandem mass spectrometry data. Proteomics. 2009; 9:1548–1555. [PubMed: 19235167]
48. Xu H, Freitas MA. A mass accuracy sensitive probability based scoring algorithm for database searching of tandem mass spectrometry data. BMC Bioinf. 2007; 8:133.
49. Guttman M, Weis DD, Engen JR, Lee KK. Analysis of overlapped and noisy hydrogen/deuterium exchange mass spectra. J Am Soc Mass Spectrom. 2013; 24:1906–1912. [PubMed: 24018862]
50. Rice P, Longden I, Bleasby A. EMBOSS: The European Molecular Biology Open Software Suite. Trends Genet. 2000; 16:276–277. [PubMed: 10827456]
51. Kelm S, Shi J, Deane CM. MEDELLER: homology-based coordinate generation for membrane proteins. Bioinformatics. 2010; 26:2833–2840. [PubMed: 20926421]
52. Lee J, Lee D, Park H, Coutsias EA, Seok C. Protein loop modeling by using fragment assembly and analytical loop closure. Proteins Struct Funct Genet. 2010; 78:3428–3436. [PubMed: 20872556]

53. Kuhlman B, Dantas G, Ireton GC, Varani G, Stoddard BL, Baker D. Design of a novel globular protein fold with atomic-level accuracy. Science. 2003; 302:1364–1368. [PubMed: 14631033]
54. Barth P, Schonbrun J, Baker D. Toward high-resolution prediction and design of transmembrane helical protein structures. Proc Natl Acad Sci USA. 2007; 104:15682–15687. [PubMed: 17905872]
55. The PyMOL Molecular Graphics System, version 1.8. Schrodinger, LLC; Portland, OR: 2015.
56. Humphrey W, Dalke A, Schulten K. VMD: visual molecular dynamics. J Mol Graphics. 1996; 14:27–38.
57. Xu H, Yang L, Freitas MA. A robust linear regression based algorithm for automated evaluation of peptide identifications from shotgun proteomics by use of reversed-phase liquid chromatography retention time. BMC Bioinf. 2008; 9:347.
58. Duc NM, Du Y, Thorsen TS, Lee SY, Zhang C, Kato H, Kobilka BK, Chung KY. Effective application of bicelles for conformational analysis of G protein-coupled receptors by hydrogen/deuterium exchange mass spectrometry. J Am Soc Mass Spectrom. 2015; 26:808–817. [PubMed: 25740347]
59. Steentoft C, Vakhrushev SY, Joshi HJ, Kong Y, Vester-Christensen MB, Schjoldager KT, Lavrsen K, Dabelsteen S, Pedersen NB, Marcos-Silva L, Gupta R, Bennett EP, Mandel U, Brunak S, Wandall HH, Levery SB, Clausen H. Precision mapping of the human O-GalNAc glycoproteome through SimpleCell technology. EMBO J. 2013; 32:1478–1488. [PubMed: 23584533]
60. Yanagawa M, Kojima K, Yamashita T, Imamoto Y, Matsuyama T, Nakanishi K, Yamano Y, Wada A, Sako Y, Shichida Y. Origin of the low thermal isomerization rate of rhodopsin chromophore. Sci Rep. 2015; 5:11081. [PubMed: 26061742]
61. Peeters MC, van Westen GJ, Li Q, IJzerman AP. Importance of the extracellular loops in G protein-coupled receptors for ligand recognition and receptor activation. Trends Pharmacol Sci. 2011; 32:35–42. [PubMed: 21075459]
62. Wheatley M, Wootten D, Conner MT, Simms J, Kendrick R, Logan RT, Poyner DR, Barwell J. Lifting the lid on GPCRs: the role of extracellular loops. Br J Pharmacol. 2012; 165:1688–1703. [PubMed: 21864311]
63. Wacker D, Wang S, McCorvy JD, Betz RM, Venkatakrishnan AJ, Levit A, Lansu K, Schools ZL, Che T, Nichols DE, Shoichet BK, Dror RO, Roth BL. Crystal Structure of an LSD-Bound Human Serotonin Receptor. Cell. 2017; 168(3):377. [PubMed: 28129538]
64. Katritch V, Cherezov V, Stevens RC. Diversity and modularity of G protein-coupled receptor structures. Trends Pharmacol Sci. 2012; 33:17–27. [PubMed: 22032986]
65. Reingruber J, Holcman D, Fain GL. How rods respond to single photons: Key adaptations of a G-protein cascade that enable vision at the physical limit of perception. BioEssays. 2015; 37:1243–1252. [PubMed: 26354340]
66. Luo DG, Yue WW, Ala-Laurila P, Yau KW. Activation of visual pigments by light and heat. Science. 2011; 332:1307–1312. [PubMed: 21659602]
67. Ahuja S, Hornak V, Yan EC, Syrett N, Goncalves JA, Hirshfeld A, Ziliox M, Sakmar TP, Sheves M, Reeves PJ, Smith SO, Eilers M. Helix movement is coupled to displacement of the second extracellular loop in rhodopsin activation. Nat Struct Mol Biol. 2009; 16:168–175. [PubMed: 19182802]
68. Ahuja S, Crocker E, Eilers M, Hornak V, Hirshfeld A, Ziliox M, Syrett N, Reeves PJ, Khorana HG, Sheves M, Smith SO. Location of the retinal chromophore in the activated state of rhodopsin*. J Biol Chem. 2009; 284:10190–10201. [PubMed: 19176531]
69. Palczewski K, Kumasaka T, Hori T, Behnke CA, Motoshima H, Fox BA, Le Trong I, Teller DC, Okada T, Stenkamp RE, Yamamoto M, Miyano M. Crystal structure of rhodopsin: A G protein-coupled receptor. Science. 2000; 289:739–745. [PubMed: 10926528]
70. Okada T, Fujiyoshi Y, Silow M, Navarro J, Landau EM, Shichida Y. Functional role of internal water molecules in rhodopsin revealed by x-ray crystallography. Proc Natl Acad Sci U S A. 2002; 99:5982–5987. [PubMed: 11972040]
71. Struts AV, Salgado GF, Tanaka K, Krane S, Nakanishi K, Brown MF. Structural analysis and dynamics of retinal chromophore in dark and meta I states of rhodopsin from 2H NMR of aligned membranes. J Mol Biol. 2007; 372:50–66. [PubMed: 17640664]

72. Chen MH, Sandberg DJ, Babu KR, Bubis J, Surya A, Ramos LS, Zapata HJ, Galan JF, Sandberg MN, Birge RR, Knox BE. Conserved residues in the extracellular loops of short-wavelength cone visual pigments. Biochemistry. 2011; 50:6763–6773. [PubMed: 21688771]
73. Coleman JL, Ngo T, Smith NJ. The G protein-coupled receptor N-terminus and receptor signalling: N-tering a new era. Cell Signalling. 2017; 33:1–9. [PubMed: 28188824]
74. Shao Z, Yin J, Chapman K, Grzemska M, Clark L, Wang J, Rosenbaum DM. High-resolution crystal structure of the human CB1 cannabinoid receptor. Nature. 2016; 540:602–606.
75. Zhang X, Stevens RC, Xu F. The importance of ligands for G protein-coupled receptor stability. Trends Biochem Sci. 2015; 40:79–87. [PubMed: 25601764]
76. Choe HW, Kim YJ, Park JH, Morizumi T, Pai EF, Krauss N, Hofmann KP, Scheerer P, Ernst OP. Crystal structure of metarhodopsin II. Nature. 2011; 471:651–655. [PubMed: 21389988]
77. Salom D, Lodowski DT, Stenkamp RE, Le Trong I, Golczak M, Jastrzebska B, Harris T, Ballesteros JA, Palczewski K. Crystal structure of a photoactivated deprotonated intermediate of rhodopsin. Proc Natl Acad Sci U S A. 2006; 103:16123–16128. [PubMed: 17060607]
78. Wang T, Duan Y. Chromophore channeling in the G-protein coupled receptor rhodopsin. J Am Chem Soc. 2007; 129:6970–6971. [PubMed: 17500517]
79. Wang T, Duan Y. Retinal release from opsin in molecular dynamics simulations. J Mol Recognit. 2011; 24:350–358. [PubMed: 21360617]
80. Piechnick R, Ritter E, Hildebrand PW, Ernst OP, Scheerer P, Hofmann KP, Heck M. Effect of channel mutations on the uptake and release of the retinal ligand in opsin. Proc Natl Acad Sci U S A. 2012; 109:5247–5252. [PubMed: 22431612]
81. Standfuss J, Edwards PC, D'Antona A, Fransen M, Xie G, Oprian DD, Schertler GF. The structural basis of agonist-induced activation in constitutively active rhodopsin. Nature. 2011; 471:656–660. [PubMed: 21389983]
82. Stenkamp RE, Filipek S, Driessen CA, Teller DC, Palczewski K. Crystal structure of rhodopsin: a template for cone visual pigments and other G protein-coupled receptors. Biochim Biophys Acta, Biomembr. 2002; 1565:168–182.
83. Riek RP, Rigoutsos I, Novotny J, Graham RM. Non-alpha-helical elements modulate polytopic membrane protein architecture. J Mol Biol. 2001; 306:349–362. [PubMed: 11237604]
84. Vaithinathan R, Berson EL, Dryja TP. Further screening of the rhodopsin gene in patients with autosomal dominant retinitis pigmentosa. Genomics. 1994; 21:461–463. [PubMed: 8088850]
85. Shah SP, Wong F, Sharp DM, Vincent AL. A novel rhodopsin point mutation, proline-170-histidine, associated with sectoral retinitis pigmentosa. Ophthalmic Genet. 2014; 35:241–247. [PubMed: 24918165]
86. Koyanagi M, Terakita A. Diversity of animal opsin-based pigments and their optogenetic potential. Biochim Biophys Acta, Bioenerg. 2014; 1837:710–716.
87. Wang C, Jiang Y, Ma J, Wu H, Wacker D, Katritch V, Han GW, Liu W, Huang XP, Vardy E, McCorvy JD, Gao X, Zhou XE, Melcher K, Zhang C, Bai F, Yang H, Yang L, Jiang H, Roth BL, Cherezov V, Stevens RC, Xu HE. Structural basis for molecular recognition at serotonin receptors. Science. 2013; 340:610–614. [PubMed: 23519210]
88. Riek RP, Finch AA, Begg GE, Graham RM. Wide turn diversity in protein transmembrane helices implications for G-protein-coupled receptor and other polytopic membrane protein structure and function. Mol Pharmacol. 2008; 73:1092–1104. [PubMed: 18202304]
89. Silvaroli JA, Arne JM, Chelstowska S, Kiser PD, Banerjee S, Golczak M. Ligand Binding Induces Conformational Changes in Human Cellular Retinol-binding Protein 1 (CRBP1) Revealed by Atomic Resolution Crystal Structures. J Biol Chem. 2016; 291:8528–8540. [PubMed: 26900151]
90. Christen M, Marcaida MJ, Lamprakis C, Aeschimann W, Vaithilingam J, Schneider P, Hilbert M, Schneider G, Cascella M, Stocker A. Structural insights on cholesterol endosynthesis: Binding of squalene and 2,3-oxidosqualene to supernatant protein factor. J Struct Biol. 2015; 190:261–270. [PubMed: 25987292]
91. Okada T, Fujiyoshi Y, Silow M, Navarro J, Landau EM, Shichida Y. Functional role of internal water molecules in rhodopsin revealed by X-ray crystallography. Proc Natl Acad Sci U S A. 2002; 99:5982–5987. [PubMed: 11972040]

92. Angel TE, Gupta S, Jastrzebska B, Palczewski K, Chance MR. Structural waters define a functional channel mediating activation of the GPCR, rhodopsin. Proc Natl Acad Sci U S A. 2009; 106:14367–14372. [PubMed: 19706523]

93. Sun X, Agren H, Tu Y. Functional water molecules in rhodopsin activation. J Phys Chem B. 2014; 118:10863–10873. [PubMed: 25166739]

94. Yuan S, Filipek S, Palczewski K, Vogel H. Activation of G-protein-coupled receptors correlates with the formation of a continuous internal water pathway. Nat Commun. 2014; 5:4733. [PubMed: 25203160]

95. Huang H, Tao YX. Functions of the DRY motif and intracellular loop 2 of human melanocortin 3 receptor. J Mol Endocrinol. 2014; 53:319–330. [PubMed: 25228159]

96. Fotiadis D, Jastrzebska B, Philippsen A, Muller DJ, Palczewski K, Engel A. Structure of the rhodopsin dimer: a working model for G-protein-coupled receptors. Curr Opin Struct Biol. 2006; 16:252–259. [PubMed: 16567090]

97. Dong C, Filipeanu CM, Duvernay MT, Wu G. Regulation of G protein-coupled receptor export trafficking. Biochim Biophys Acta, Biomembr. 2007; 1768:853–870.

98. Zheng H, Loh HH, Law PY. Posttranslation modification of G protein-coupled receptor in relationship to biased agonism. Methods Enzymol. 2013; 522:391–408. [PubMed: 23374194]

99. Zhu L, Jang GF, Jastrzebska B, Filipek S, Pearce-Kelling SE, Aguirre GD, Stenkamp RE, Acland GM, Palczewski K. A naturally occurring mutation of the opsin gene (T4R) in dogs affects glycosylation and stability of the G protein-coupled receptor. J Biol Chem. 2004; 279:53828–53839. [PubMed: 15459196]

100. Murray AR, Vuong L, Brobst D, Fliesler SJ, Peachey NS, Gorbatyuk MS, Naash MI, Al-Ubaidi MR. Glycosylation of rhodopsin is necessary for its stability and incorporation into photoreceptor outer segment discs. Hum Mol Genet. 2015; 24:2709–2723. [PubMed: 25637522]

Abbreviations

CB1	cannabinoid receptor 1
DDM	*n*-dodecyl *β*-D-maltopyr-anoside
EL	extracellular loop
GPCR	G protein-coupled receptor
H/D	hydrogen-deuterium
IL	intracellular loop
L/LWS	long wavelength sensitive opsin 1
MS	mass spectrometry
M/LWS	medium wavelength sensitive opsin 1 or green opsin
NMR	nuclear magnetic resonance spectroscopy
RMSD	root-mean-square deviation
TM	transmembrane helix
SDS-PAGE	sodium dodecyl sulfate-polyacrylamide gel electrophoresis
SEC	size exclusion chromatography

SWS1	short wavelength sensitive opsin 1
5-HT$_{1B}$	5-hydroxytryptamine receptor 1B
5-HT$_{2B}$	5-hydroxytrypta mine receptor 2B

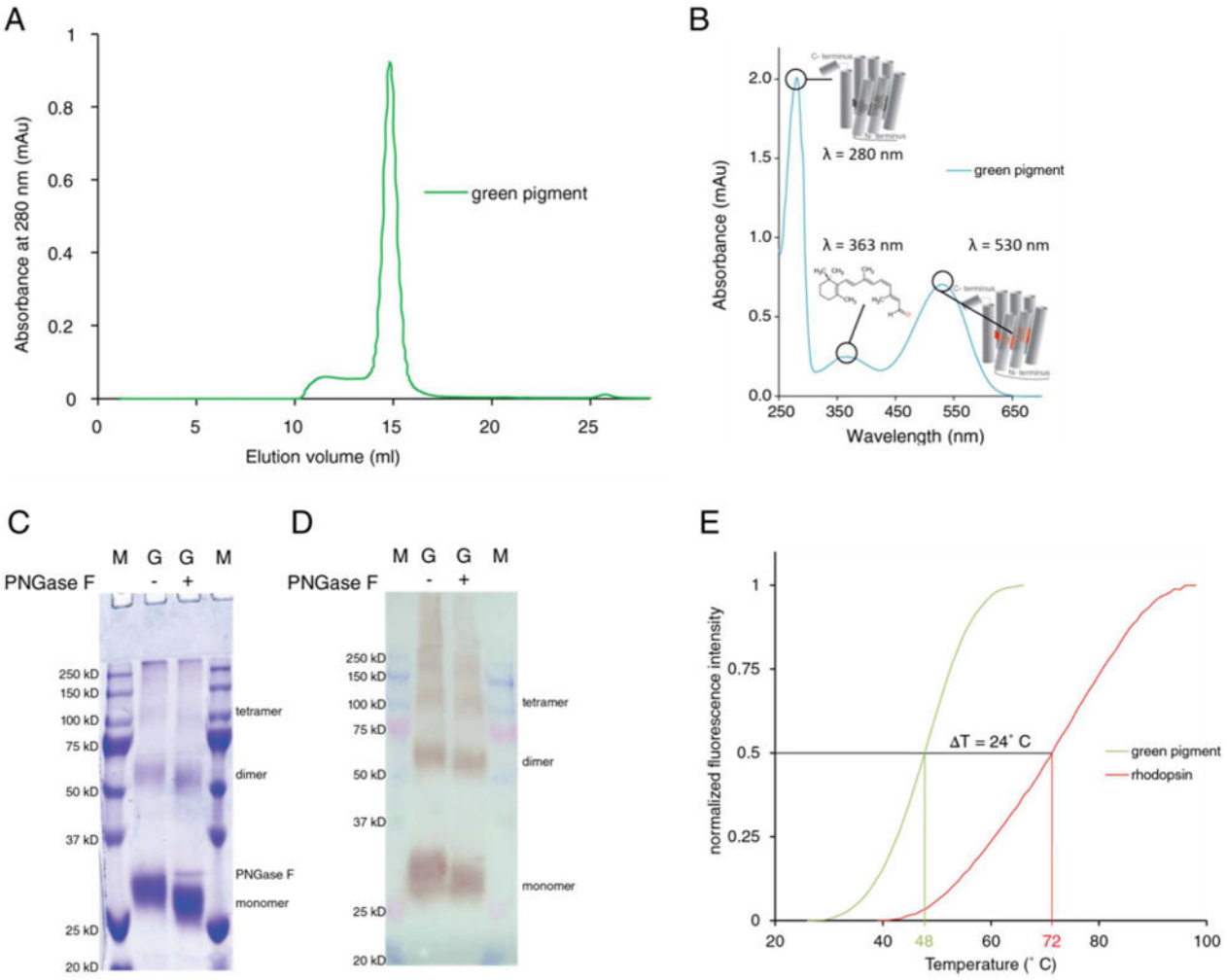

Figure 1.

Purification of green opsin by size exclusion chromatography and analysis of glycosylation by SDS-PAGE and immunoblotting. Panel A is a size exclusion chromatogram as obtained from numerous purifications. It reveals that aggregates and oligomers eluted in fraction 11 whereas dimeric opsin eluted in fractions 12–18 (see also Figure S1). The 1D4 peptide used for affinity chromatography eluted in fraction 25. Panel B shows the absorbance measurements of fraction 15. The peak at 530 nm originates from the chromophore bound to green opsin; the absorbance at 363 nm is due to free retinal in the buffer, and the 280 nm absorbance results from aromatic amino acid residues Trp, Tyr, and Phe. These absorbance spectra are routinely applied to verify the purity and yield of the expressed pigment. Panel C shows Coomassie staining of glycosylated (lane 2) and deglycosylated (lane 3) opsin. Following PNGase F treatment, the deglycosylated receptor undergoes a mobility shift toward a molecular weight lower than that of the glycosylated receptor. Additionally, lane 3 reveals a thin band attributed to PNGase F at ~32 kDa. Panel D displays immunoblotting analysis of the glycosylated (lane 2) and deglycosylated (lane 3) opsin. The monomer (30 kDa), dimer (60 kDa), tetramer (120 kDa), and higher oligomeric species can be detected by both SDS-PAGE and immunoblotting analyses. Lanes 1 and 4 in both panels contain protein

markers. Panel E displays triplicate differential scanning fluorescence measurements of green opsin and bovine rhodopsin. The normalized fluorescence of green opsin (green line) was fitted to the Boltzmann equation (R = 0.9998, and R_{sqr} = 0.9997) that resulted in a melting temperature of 48 ± 0.06 °C. The corresponding temperature obtained for bovine rhodopsin (red line) (R = 0.9988, and R_{sqr} = 0.9976) revealed a melting temperature of 72 ± 0.28 °C. The difference between the two melting temperatures is 24 ± 0.29 °C.

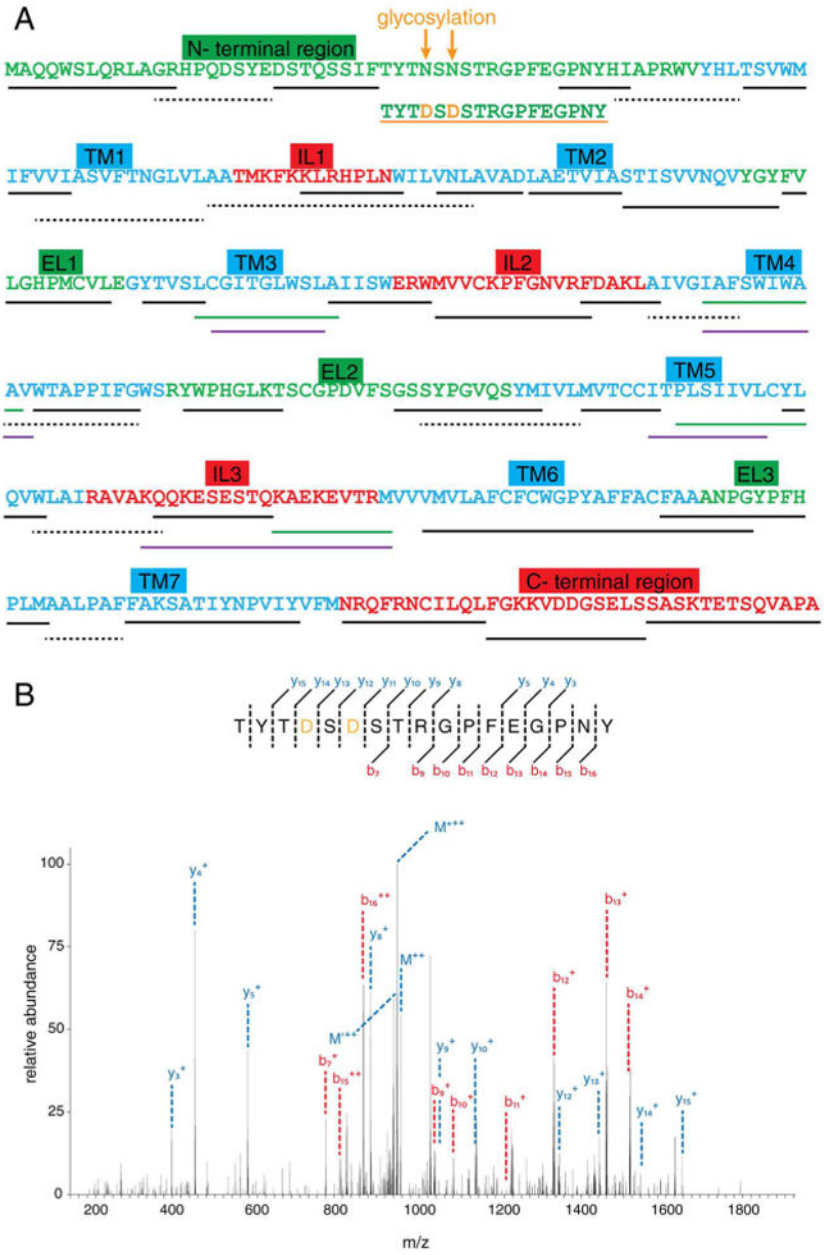

Figure 2.

Sequence, glycosylation, and peptide coverage of the green opsin construct by MS. Only peptides with a significant score with a p value of <0.05 were selected and further analyzed in triplicate. (A) Glycosylation sites are colored orange. The extracellular side of the receptor is colored green; the cytosolic domain is colored red, and the transmembrane domains are colored blue. Black lines indicate the peptide coverage in H_2O and D_2O, in both dark and bleached states. In the case of overlapping peptides, the percentage of H/D exchange applied is shown with a solid line. For gaps in the coverage, the missing percentage was derived from peptides with a dashed line. The green line indicates coverage only in the D_2O dark state, and the violet line displays peptide coverage found only in the D_2O bleached state. (B) MS/MS spectrum of the N-terminal peptide, residues 29–45.

Residues N32 and N34 were detected as D32 and D34, respectively. The sequence is displayed above the spectrum, and the two glycosylated residues are colored orange. The b and y ions are colored red and blue, respectively. The M notation refers to the molecular ion.

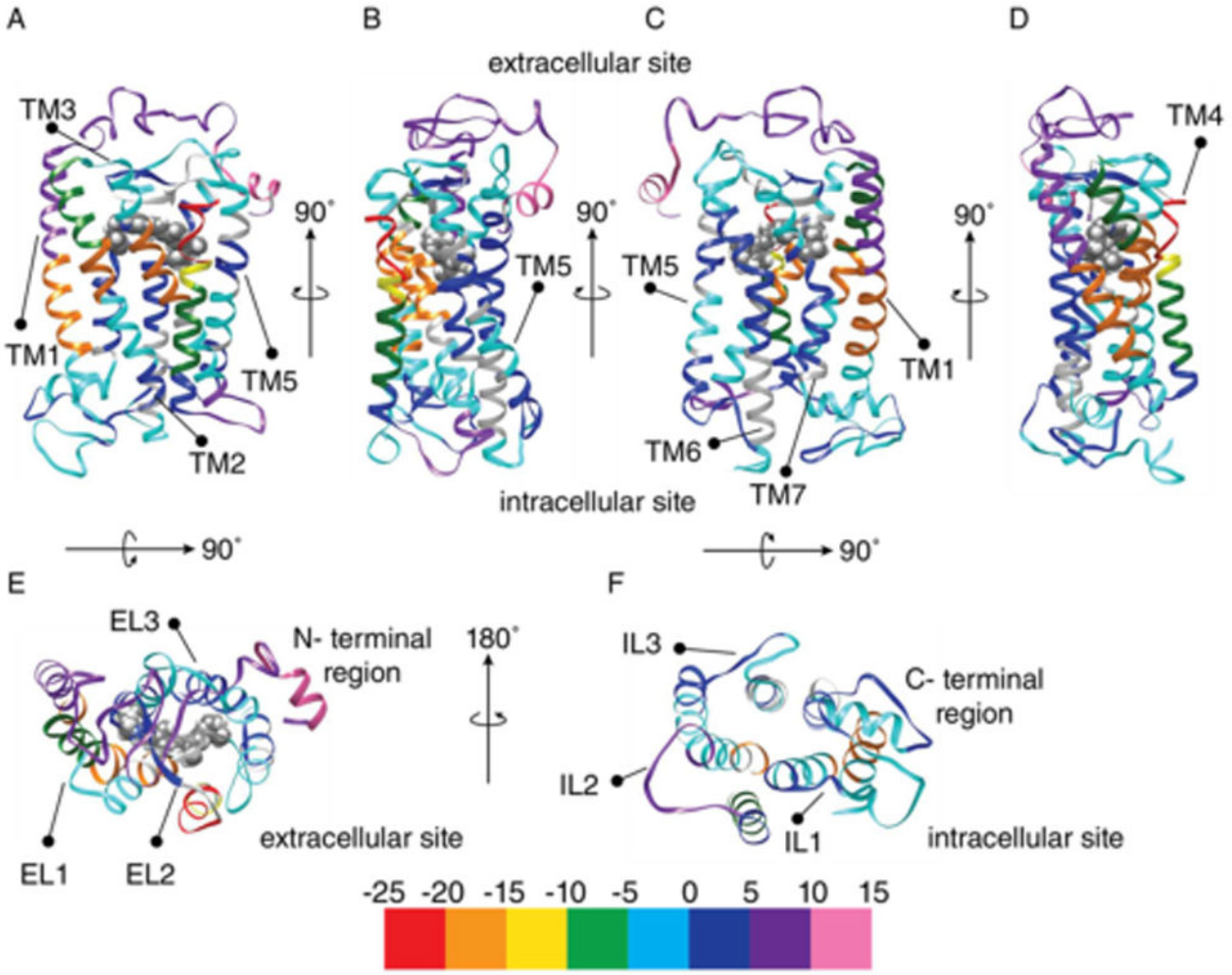

Figure 3.

H/D exchange difference map of green opsin in the dark and bleached states. The percent deuteration of the dark state was subtracted from the percent deuteration of the bleached state and displayed on the surface of the receptor. Positive differences in percent deuteration between states [$\Delta\%_{deuteration}$ (dark–bleached)] are color-coded as follows: blue for 0–4%, violet for 5–9%, and pink for 10–14%. Negative differences of percent deuteration are color coded as follows: cyan for 0–4%, green for 5–9%, yellow for 10-14%, orange for 15–19%, and red for 20–24%. Undefined regions are colored gray. Panels A–D represent side views of the green pigment, and panels E and F show top and bottom views, respectively.

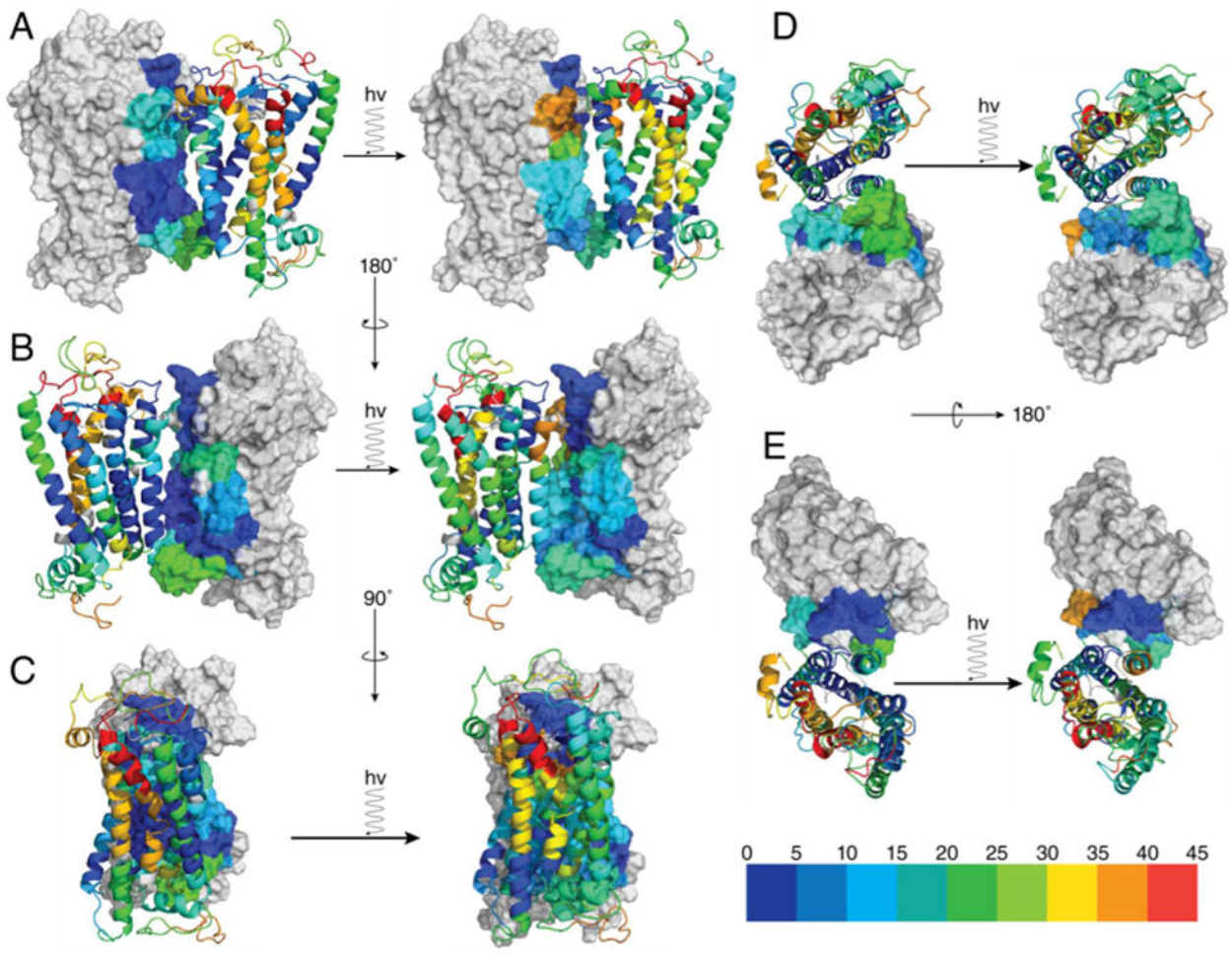

Figure 4.

Dimer interface analysis of dark and bleached states of green opsin. Panels A–C show side views of the green dimer in the dark and bleached states. Panels D and E show bottom and top views of the green dimer in the dark and bleached states, respectively. In all panels, the dimer in the dark state is shown on the left while the dimer in the bleached state is shown on the right. One monomer is displayed in a cartoon representation and the second monomer as a surface. Both the cartoon and surface representations show the dimer interface color-coded according to H/D exchange as follows: dark blue for 0–4%, light blue for 5–9%, cyan for 10–14%, cadet blue for 15–19%, green for 20–24%, light green for 25–29%, yellow for 30–34%, orange for 35–39%, and red for 40–44%. Undefined regions are colored gray.

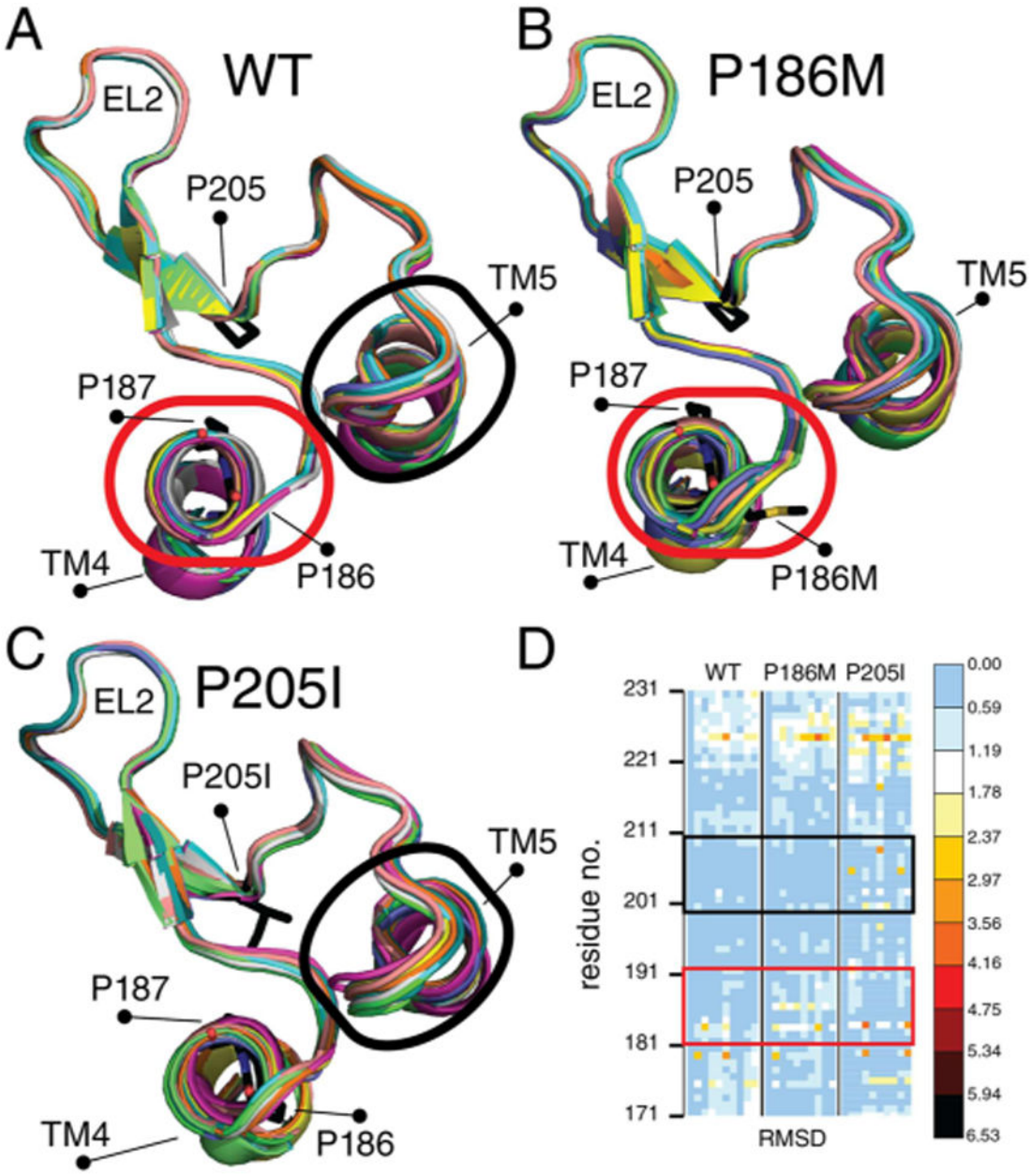

Figure 5.

Structural models and RMSD analysis of EL2 in WT green opsin and its P186M and P205I substitutions. The 10 energetically favored structures were aligned and are displayed as cartoons from residue 180 to 224. (A) The Pro-Pro motif in the WT green opsin is highlighted with a red oval. The black oval indicates the region of variation in the structure caused by the P205I mutation. (B) Structures resulting from the P186M mutation. The red oval indicates a major variation in structure induced by the mutation (compare with the red oval region in panel A). (C) Major variations in structure are caused by the P205I mutation (black oval; compare to the black oval region in panel A). (D) Heat map of RMSD analysis of the 10 energetically favored structures shown in panels A–C. The red and black rectangles correspond to the ovals displayed in A–C.

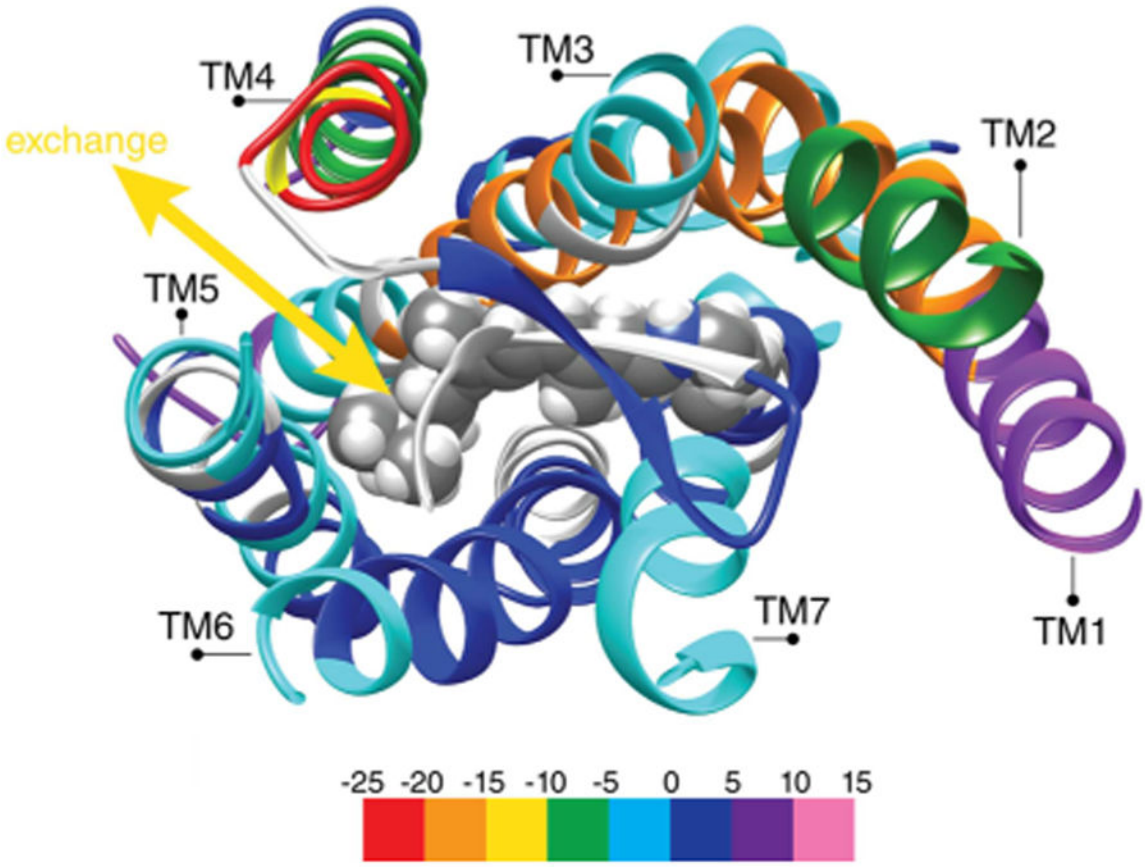

Figure 6.

All-*trans*-retinal exit pathway near the extracellular side of green opsin. The retinylidene Schiff base and K312 are represented by spheres. H/D exchange of the dark state was subtracted from that of the bleached state, and the difference is displayed on TMs shown as a cartoon. H/D exchange itself is color-coded as follows: dark blue for 0–4%, light blue for 5–9%, cyan for 10–14%, cadet blue for 15–19%, green for 20–24%, light green for 25–29%, yellow for 30–34%, orange for 35–39%, and red for 40–44%. Undefined regions are colored gray. A possible exchange route for water or all-*trans*-retinal is indicated with a yellow arrow.